K. Gadeyne
T. Lefebvre
H. Bruyninckx

Department of Mechanical Engineering
Katholieke Universiteit Leuven
Celestijnenlaan 300B, 3001 Leuven, Belgium
herman.bruyninckx@mech.kuleuven.be

Bayesian Hybrid Model–State Estimation Applied to Simultaneous Contact Formation Recognition and Geometrical Parameter Estimation

Abstract

In this paper we describe a Bayesian approach to model selection and state estimation for sensor-based robot tasks. The approach is illustrated with a hybrid model–state estimation example from force-controlled autonomous compliant motion: simultaneous (discrete) contact formation recognition and estimation of (continuous) geometrical parameters. Previous research in this area mostly tries to solve one of the two subproblems, or treats the contact formation recognition problem separately, avoiding integration between the solutions to the contact formation recognition and the geometrical parameter estimation problems. A more powerful hybrid model, explicitly modeling contact formation transitions, is developed to deal with larger uncertainties. This paper demonstrates that Kalman filter variants have limits: iterated extended Kalman filters can only handle small uncertainties on the geometrical parameters, while the non-minimal state Kalman filter cannot deal with model selection. Particle filters can handle the increased level of model complexity. Explicit measurement equations for the particle filter are derived from the implicit kinematic and energetic constraints. The experiments prove that the particle filter approach successfully estimates the hybrid joint posterior density of the discrete contact formation variable and the 12-dimensional, continuous geometrical parameter vector during the execution of an assembly task. The problem shows similarities with the well-known problems of data association in simultaneous localization and map-building (SLAM) and model selection in global localization.

The International Journal of Robotics Research
Vol. 24, No. 8, August 2005, pp. 615-630,
DOI: 10.1177/0278364905056196

KEY WORDS—Bayesian model selection, state estimation, sensor-based robot tasks, autonomous compliant motion, simultaneous contact formation recognition and estimation of geometrical parameters, data association, SLAM, particle filter, hybrid joint density

1. Introduction

Compliant motion tasks (De Schutter and Van Brussel 1988) are tasks in which a robot manipulates a tool or work piece in contact with the environment. In industrial environments, compliant motion tasks are often position-controlled and hence require structured environments (i.e., the work pieces are accurately positioned and their dimensions are known), and/or (instrumented) passive compliances. The presented research increases the robot's autonomy for "one-off" compliant tasks in less structured environments, e.g., deburring of cast pieces without expensive fixtures, assembly, maintenance and autonomous manipulation skills in teleoperation, etc.

Figure 1 shows the execution of the particular autonomous compliant motion task whose experimental data are illustrated later in the paper. A robot manipulator, equipped with a force sensor, should insert a cube—hereafter in this paper referred to as a manipulated object (MO)—into a "corner" (environment object (EO)). Both the location of the MO (with respect to the end effector of the robot) and the EO (with respect to the environment), and some dimensions of the MO/EO are uncertain. These variables are referred to as the geometrical parameters, and they form the continuous part of the estimation problem.[1]

1. In this paper we use the term "parameter" in the sense of a static state.

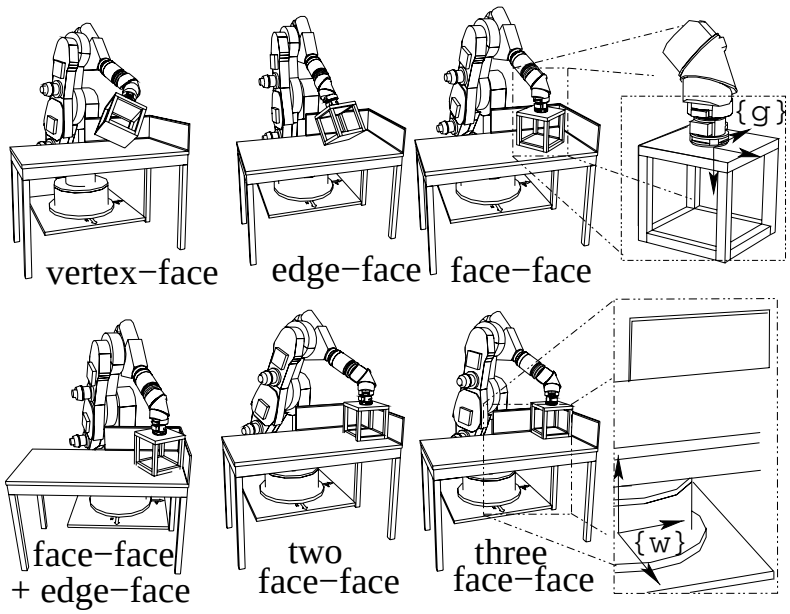

Fig. 1. Execution of the "cube-in-corner" autonomous compliant motion experiment: different CFs.

The location of the end effector with respect to the world frame is assumed to be known, i.e., the uncertainty due to the kinematic chain of the robot manipulator (calibration errors, backlash, etc.) is negligible compared to the uncertainty on the geometrical parameters. The measurements used for the estimation are wrenches (forces and torques) from a wrist force sensor, and position measurements from the encoders.

The execution of a typical task can be segmented into different discrete contact formations (CFs; e.g., a vertex–plane contact, an edge–plane contact or a plane–plane contact): every CF gives rise to a different measurement model. In order to be able to estimate the geometrical parameters during the force-controlled execution of CF sequences, it is thus necessary to recognize the current CF. The problem of CF recognition includes the simpler problem of CF transition detection. Lefebvre, Bruyninckx, and De Schutter (2003a) describe both the problem formulation and measurement equations of the presented autonomous compliant motion case.

A Bayesian estimator recognizes a contact transition by the statistical inconsistency of the measurements with the current measurement model, i.e., consecutive measurements no longer "fit" into the measurement model and this cannot be explained by the modeled uncertainties on the measurements or on the parameters in the model. For example, when a contact is gained, the wrench measurements are inconsistent with the previous measurement equations, so that a wrench is measured in a direction of motion freedom; when a contact is lost, the twist measurements are inconsistent with the motion freedom allowed by the contact model.

Compared to previous research (Lefebvre, Bruyninckx, and De Schutter 2003a), the presented work allows the execution of the task with larger uncertainty. Indeed, previous research assumes that whenever a contact state transition is detected by a statistical consistency test on the wrench measurements, the next CF is known. However, if the initial uncertainty on the geometrical parameters is large, there are many possible next CFs. This work develops a hybrid (partly discrete, partly continuous) approach, using an explicit discrete model for CF transitions where both pose and wrench measurements are used to detect CF transitions. We argue that Kalman filter variants cannot cope with the more powerful hybrid models introduced in this work to deal with this increased uncertainty, but we show that particle filters can. The uncertainty the robot can cope with is only limited by the number of particles, the chosen proposal distribution and problem specific optimizations of the particle filter algorithm. However, a particle filter needs explicit measurement equations, and this paper shows how to transform available implicit measurement equations (kinematic closure and energy dissipation) into explicit ones.

The outline of this paper is as follows. In Section 2 we describe previous work in the fields of geometrical parameter estimation, CF transition monitoring and recognition or combinations of both. The hybrid joint posterior density is derived in a formal way in Section 3. In Section 4 we describe why Kalman filter variants, used extensively in previous research, are not able to deal with the developed model. Particle filters can deal with the extra amount of complexity. The hybrid

model is also compared to the models used in probabilistic mobile robotics. In Section 5 we describe the measurement equations for the cube-in-corner assembly task and we explain what it takes to use a particle filter to represent the hybrid joint posterior. The results of the estimation using a particle filter approach are described in Section 6, and in Section 7 we give an overview of the software framework used for the implementation. The paper ends with some conclusions and directions for future work.

2. Previous Work

Most authors consider only one of the two problems, or do not model the interaction between the CF states and the geometrical parameters.

Estimation of Geometrical Parameters. The identification of the contact location and orientation based on wrench, position and/or twist measurements is often applied for single point–surface contacts. The main application area is two-dimensional (2D) contour tracking. Only a few authors consider contact situations which are more general than point–surface contacts (Mimura and Funahashi 1994; De Schutter et al. 1999; Debus, Dupont, and Howe 2002). Most authors use non-recursive deterministic estimation, i.e., the estimates are based only on the last measured data and no measurement uncertainties are considered.

CF Transition Monitoring and Recognition. CF recognition techniques can be divided into methods based on learned contact models and methods based on analytical contact models. The learned models can handle uncertainty taken into account at modeling time, i.e., deviations from parameter values for which training data were available. A deterministic, Bayesian, fuzzy (Skubic and Volz 2000) or neural network (Asada 1993) model performs the CF recognition or transition detection. Hidden Markov models (HMMs; Hannaford and Lee 1991; Hovland and McCarragher 1998) are a popular tool for both the detection of transitions and the recognition of the current CF.

Simultaneous CF Recognition and Geometrical Parameter Estimation. CF models are a function of the uncertain geometrical parameters. During task execution, the uncertainty reduces due to the sensor information. This increases the knowledge of the "true state" of the system and environment, which improves the force control, the CF transition monitoring, and the CF recognition.

Mimura and Funahashi (1994) recognize vertex–plane, edge–plane, and plane–plane CFs based on wrench, twist, and pose measurements. The different CF models are tested from the least to the most constrained until a model is found which is consistent with the data (i.e., a model for which the geometrical parameters can be determined).

In our lab, for execution of the cube-in-corner task with small uncertainties, the executed sequence of CFs is assumed to be error-free, i.e., after a contact transition the CF is the next one in the (off-line calculated) task plan (Hirukawa, Papegay, and Matsui 1994; Xiao and Ji 2001). This means that after an inconsistency detection two CFs are probable: the same CF as before the inconsistency detection (false alarm) and the next CF in the task plan. This is only valid for small uncertainties. De Schutter et al. (1999) and Lefebvre, Bruyninckx, and De Schutter (2003a, 2004) estimate the geometrical parameters with Kalman filters and detect inconsistency using an SNIS-test (Bar-Shalom and Li 1993). Eberman (1997) has already presented a similar approach for linear contact models, using a maximum likelihood approach. Several Bayesian techniques such as Kalman filter variants (Kalman 1960; Lefebvre, Bruyninckx, and De Schutter 2003b) and Monte Carlo methods (Doucet, de Freitas, and Gordon 2001; Gadeyne and Bruyninckx 2001) have been used for the estimation of the geometrical parameters, assuming the CF is known. These approaches only use measurement information for the detection of a CF transition, and do not develop an explicit model for CF transitions. In Mihaylova et al. (2002), a first step towards a multiple model posterior is made.

Debus, Dupont, and Howe (2002) present similar results with deterministic multiple model estimation based on pose measurements. The penetration distances of the objects from the different deterministic filters (CFs) are used as measurements in a HMM which has CFs as states. Their HMM approach, although using only deterministic penetration distances (and not the information from the wrenches) as measurements, is similar to the simplified system model of the hybrid joint posterior developed in Section 3.

Recently, Slaets et al. (2004) have presented some results in which a Bayes' factor approach is applied in combination with an SNIS-test. Their method is more oriented to model building from a given number of primitives, and the results they obtain are only valid once the posterior has converged to a unimodal Gaussian.

3. Bayesian Estimation of the Hybrid Joint Density

The autonomous execution—without assuming the CF sequence is known—of the experiment of Figure 1 requires a hybrid (partly continuous, partly discrete) joint posterior probability density function (PDF) representing the belief that, at time-step k, the CF is j ($0 \leq j < \#CFs$) and the geometrical parameters $\boldsymbol{X}$ have a certain value $\boldsymbol{x}$, given all measurements $\boldsymbol{Z}$ up to k

$$P\left(\boldsymbol{X} = \boldsymbol{x}, CF_k = j \mid \boldsymbol{Z}_{1\ldots k} = z_{1\ldots k}\right), \tag{1}$$

where $\boldsymbol{Z}_{1\ldots k} = \boldsymbol{Z}_1, \ldots, \boldsymbol{Z}_k$.[2] For the ease of notation, we will shorten $\boldsymbol{A} = \boldsymbol{a}$ into $\boldsymbol{a}$ wherever the distinction between a stochastic variable and a concrete value is unambiguous.

2. Capitals denote probability variables and lowercase letters denote concrete values.

Figure 2 shows an example of such a hybrid joint posterior density, if $\boldsymbol{X}$ would be one-dimensional. Each CF j has "its own" continuous density $P\,(x \mid CF_k = j, \boldsymbol{z}_{1\ldots k})$. The difference between $P\,(x \mid CF_k = j, \boldsymbol{z}_{1\ldots k})$ and $P\,(x, CF_k = j \mid \boldsymbol{z}_{1\ldots k})$ is only a scalefactor independent of $\boldsymbol{x}$ (product rule).

In many sensor-based tasks, including the particular case of the above-mentioned assembly, there is no obvious model-based (direct) relation $P(\boldsymbol{z}_k \mid CF_k)$ between the discrete model and the measurements of the sensor. So, one cannot use Bayes' rule to find out how much information one has already gathered to support a particular CF:

$$P\,(CF_k \mid \boldsymbol{z}_{1\ldots k}) = \frac{P\,(\boldsymbol{z}_k \mid CF_k)\,P\,(CF_k \mid \boldsymbol{z}_{1\ldots k-1})}{P\,(\boldsymbol{z}_k \mid \boldsymbol{z}_{1\ldots k-1})}.$$

However, a measurement model $P(\boldsymbol{z}_k \mid \boldsymbol{x}, CF_k = j)$ does exist: given the current CF and the geometrical parameters, we know the probability that a certain measurement of the force sensor will occur.

Assuming a Markovian system, Bayes' rule allows us to update the joint hybrid posterior eq. (1) recursively with each new measurement $\boldsymbol{z}_k$. The following derivation makes this explicit for the hybrid PDF $P(\boldsymbol{x}, CF_k = j \mid \boldsymbol{z}_{1\ldots k})$. The derivation applies to any hybrid dynamical system, but assumptions about the specific nature of the CF recognition and geometrical parameter estimation allow us to simplify some of the general expressions. Applying Bayes' rule to (1) yields:

$$\begin{aligned} &P\,(\boldsymbol{x}, CF_k = j \mid \boldsymbol{z}_{1\ldots k}) \\ &= \frac{P\,(\boldsymbol{z}_k \mid \boldsymbol{x}, CF_k = j)\,P\,(\boldsymbol{x}, CF_k = j \mid \boldsymbol{z}_{1\ldots k-1})}{P\,(\boldsymbol{z}_k \mid \boldsymbol{z}_{1\ldots k-1})}. \end{aligned} \tag{2}$$

$P\,(\boldsymbol{x}, CF_k = j \mid \boldsymbol{z}_{1\ldots k-1})$ is often called the prediction density. It describes our belief about the hybrid state $(\boldsymbol{X}, CF_k)$ at time-step k, without taking into account the information provided by the measurement at that time.

The prediction density $P\,(\boldsymbol{x}, CF_k = j \mid \boldsymbol{z}_{1\ldots k-1})$ is related to the posterior at time-step $k-1$ by a hybrid system model:

$$\begin{aligned} &P\,(\boldsymbol{X} = \boldsymbol{x}, CF_k = j \mid \boldsymbol{z}_{1\ldots k-1}) \\ &= \sum_i \int_{\boldsymbol{x}'} P\left(\boldsymbol{X} = \boldsymbol{x}, CF_k = j \mid \boldsymbol{X} = \boldsymbol{x}', CF_{k-1} = i\right) \\ &\quad P\left(\boldsymbol{X} = \boldsymbol{x}', CF_{k-1} = i \mid \boldsymbol{z}_{1\ldots k-1}\right) \mathrm{d}\boldsymbol{x}'. \end{aligned} \tag{3}$$

The product rule applied to the conditional PDF describing the system update yields

$$\begin{aligned} &P\left(\boldsymbol{X} = \boldsymbol{x}, CF_k = j \mid \boldsymbol{X} = \boldsymbol{x}', CF_{k-1} = i\right) \\ &\quad = P\left(\boldsymbol{X} = \boldsymbol{x} \mid CF_k = j, \boldsymbol{X} = \boldsymbol{x}', CF_{k-1} = i\right) \\ &\quad \times P\left(CF_k = j \mid \boldsymbol{X} = \boldsymbol{x}', CF_{k-1} = i\right). \end{aligned}$$

In the particular case of simultaneous CF recognition and geometrical parameter estimation, the first term of this product simplifies to $\delta(\boldsymbol{x} - \boldsymbol{x}')$ ($\delta(\boldsymbol{x})$ denotes the Dirac function) since $\boldsymbol{X}$ is a static variable (parameter): the estimate about where the MO and EO are located does not change under a change of CF assumption.

The last term $P(CF_k = j \mid \boldsymbol{X} = \boldsymbol{x}', CF_{k-1} = i)$ is the probability of a contact transition, given knowledge about the current CF and given that the value of $\boldsymbol{X} = \boldsymbol{x}'$. Indeed, using the information of the velocity setpoints sent to the motion controller, we can predict CF transitions using the forward kinematics of the robot manipulator. However, the current implementation of the system model only uses an off-line calculated graph (Hirukawa, Papegay, and Matsui 1994; Xiao and Ji 2001), to describe the possible transitions between CFs:

$$\begin{aligned} &P\left(CF_k = j \mid \boldsymbol{X} = \boldsymbol{x}', CF_{k-1} = i\right) \\ &\quad \approx P\,(CF_k = j \mid CF_{k-1} = i)\,. \end{aligned} \tag{4}$$

This simplification has some disadvantages, because it does not correspond well to reality. Indeed, using this model, the probability of remaining in a certain CF decreases exponentially with time:[3]

$$P\,(CF_{\tau+1\ldots\tau+k} = [j, \ldots, j] \mid CF_\tau = j) = a_{jj}^k,$$

while, in reality, the probability of remaining in a certain CF depends also on the value of the geometrical parameter vector and the speed of the end effector. The above-mentioned graph only specifies which CF transitions are possible, and does not yield probabilities a_{ij}. However, the experiment described in Section 6 shows that the information contained in the measurements is rich enough to compensate this poor system model and the chosen values for the parameters a_{ij} are not critical for obtaining good results.

Note that another way to cope with the issue of CF transition models is to use model building from scratch. Slaets et al. (2004) detect several vertex–plane contacts and use hypothesis tests to identify if, for example, two (or more) vertices are in contact with the same plane. This approach does not need the above-described CF transition model $P(CF_k = j \mid X = x, CF_{k-1} = i)$. However, the results of the hypothesis tests are only valid once the posterior has converged to a unimodal Gaussian.

So, for the autonomous compliant motion case, taking into account assumption (4), eq. (3) becomes

$$\begin{aligned} &P\,(\boldsymbol{X} = \boldsymbol{x}, CF_k = j \mid \boldsymbol{z}_{1\ldots k-1}) \\ &\quad \approx \sum_i \int_{\boldsymbol{x}'} \delta(\boldsymbol{x} - \boldsymbol{x}')P(CF_k = j \mid CF_{k-1} = i) \\ &\qquad P\left(\boldsymbol{X} = \boldsymbol{x}', CF_{k-1} = i \mid \boldsymbol{z}_{1\ldots k-1}\right) \mathrm{d}\boldsymbol{x}' \\ &\quad = \sum_i \big[P(CF_k = j \mid CF_{k-1} = i) \\ &\qquad P\,(\boldsymbol{X} = \boldsymbol{x}, CF_{k-1} = i \mid \boldsymbol{z}_{1\ldots k-1})\big]. \end{aligned} \tag{5}$$

3. $[j, \ldots, j]$ denotes a sequence of k j's.

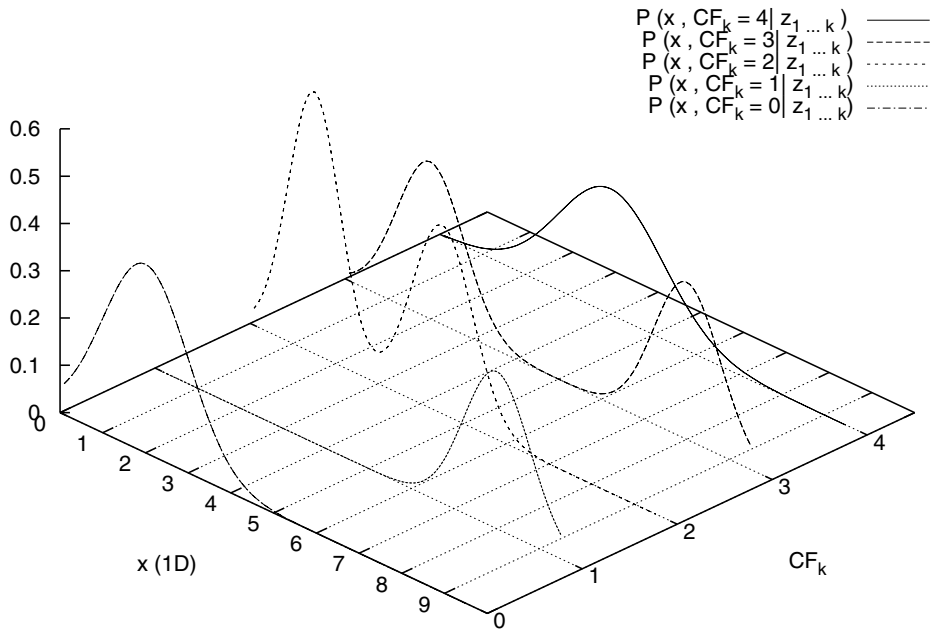

Fig. 2. Example of a hybrid joint density, with a one-dimensional geometrical parameter $\boldsymbol{X}$. The CF_k axis represents the CF at time-step k.

$P\,(\boldsymbol{X} = \boldsymbol{x}, CF_{k-1} = i \mid z_{1\ldots k-1})$ represents the posterior density at time $k-1$.

4. Interpretation and Discussion

Equations (2) and (5) describe the recursive two-step system and measurement update of the Bayesian joint hybrid posterior for semidynamic[4] systems:

System update:

$$P\,(\boldsymbol{x}, CF_k = j \mid z_{1\ldots k-1}) = \sum_i P(CF_k = j \mid CF_{k-1} = i)$$

$$P\,(\boldsymbol{x}, CF_{k-1} = i \mid z_{1\ldots k-1})\,;$$

Measurement update:

$$P\,(\boldsymbol{x}, CF_k \mid z_{1\ldots k}) \sim P\,(z_k \mid \boldsymbol{x}, CF_k)\,P\,(\boldsymbol{x}, CF_k \mid z_{1\ldots k-1})\,. \tag{6}$$

The system update describes each prediction density as a weighted sum of the different continuous estimates for each CF at time $k-1$, where the weights $P(CF_k = j \mid CF_{k-1} = i)$ include information from a system graph. At each time-step, every continuous density in Figure 2 is replaced by a weighted sum of the N previous estimates (N represents the number of CFs).

4. We use the term semidynamic since the CF model is dynamic, but the geometrical parameters are static.

Given the joint posterior (1), it is straightforward to estimate the current probability distribution over CFs, via marginalization of the geometrical parameters:

$$P\,(CF_k = j \mid z_{1\ldots k}) = \int_x P\,(\boldsymbol{x}, CF_k = j \mid z_{1\ldots k})\;\mathrm{d}\boldsymbol{x}. \tag{7}$$

The marginal probability that the geometrical parameter vector $\boldsymbol{X}$ has a value $\boldsymbol{x}$, is expressed as a weighted average over the state estimates of the different CFs:

$$P\,(\boldsymbol{x} \mid z_{1\ldots k}) = \sum_i P\,(\boldsymbol{x}, CF_k = i \mid z_{1\ldots k})\,. \tag{8}$$

As with all Bayesian algorithms, several implementations of the above derivation could be used, at least in theory. In Section 4.1 we describe why Kalman filter variants (Lefebvre, Bruyninckx, and De Schutter 2003a, 2004), used in previous research to estimate the geometrical parameters assuming the CF is known, are not capable of dealing with the more powerful model as described by eq. (6). Particle filters (Gordon, Salmond, and Smith 1993; Doucet, de Freitas, and Gordon 2001) can deal with the extra complexity introduced by the hybrid model and are described in Section 4.2.

In Section 4.3 we describe some analogies and differences between simultaneous CF recognition and geometrical parameter estimation and simultaneous localization and map-building (SLAM) problems in mobile robotics.

4.1. Kalman Filter Variants

The interaction between the estimates from the different CFs—necessary for coping with extra uncertainty introduced by the fact that CFs are unknown—results in an increasing complexity of the posteriors shape with time. If, at time 0, we start with N unimodal Gaussians, at time-step k, eq. (1) consists of N multimodal Gaussians with N^{k-1} modes, resulting in memory requirements that are quadratic with time. Hence, we have to eliminate most of the modes at each time-step to maintain a constant complexity. However, the resulting PDF should be a consistent and informative approximation (Lefebvre 2003) of the original density. A variety of algorithms have been developed to perform this reduction in the linear Gaussian case: e.g., second-order generalized pseudo-Bayes (GPB2), interacting multiple model filtering (IMM), etc.. They are sometimes referred to as assumed density filtering (ADF; see, for example, Bar-Shalom and Fortmann 1988 or http://www.stat.cmu.edu/∼minka/dynamic.html for an overview).

4.1.1. Application to Cube-in-Corner Assembly

Unfortunately, for the assembly problem described in this paper, the measurement model—given a certain contact formation—$P(\boldsymbol{z}_k \mid \boldsymbol{x}, CF_k)$ is still non-linear. Previous research focused on Kalman filter variants, and has used the iterated extended Kalman filter (IEKF) to solve the problem of estimating the geometrical parameters, given a certain CF (Lefebvre, Bruyninckx, and De Schutter 2003a). This limits the execution of the task to execution under relatively small uncertainties due to the linearization. To allow the execution of the experiment under large uncertainties, the non-minimal state Kalman filter (NMSKF; Lefebvre, Bruyninckx, and De Schutter 2005) was developed. By transforming the geometrical parameters into a higher-dimensional space where a linear model is obtained, and solving the estimation problem in that space, this filter avoids the accumulation of errors due to linearization. However, a different transformation is used for each CF. This means that the multiple model approach cannot be applied in the higher-dimensional space. Therefore, in the case of the presented non-linear measurement models, Kalman filter variants are not capable of dealing with the increased complexity of the hybrid joint posterior.[5]

4.2. Particle Filter Approaches

The Particle filter (Doucet, de Freitas, and Gordon 2001) is another possibility to perform inference in this hybrid model. Indeed, sequential Monte Carlo[6] methods use a fixed number of samples to represent an arbitrary complex PDF. Contrary to Kalman filter variants, particle filters can easily track discrete, continuous and hybrid random variables. Furthermore, their ability to track multimodal posteriors and to cope with non-linear measurement equations makes them attractive to use for inference in hybrid non-linear models. However, they have also several disadvantages with respect to Kalman filters. Their computational complexity is significantly higher than that of Kalman filter derivatives, especially in this case where the state vector is 12-dimensional (or even higher if some of the dimensions of the objects are unknown). In particular cases, combined analytical–sample-based techniques (Rao–Blackwellization; Murphy and Russell 2001; Montemerlo et al. 2002) can reduce this complexity.

Since particle filters use a discrete approximation of the posterior density, they are also more sensitive to outliers. When there is an outlier present, particle weights are very unevenly distributed, and it takes many samples to obtain a "good" estimate of the true posterior density. A similar problem occurs with very accurate measurement models. As illustrated in Figure 3, the basic particle filter algorithm does not always deal very well with "sharp" likelihood functions. A good choice of the proposal density can often be of great help to avoid this degeneracy problem. Doucet, Godsill, and Andrieu (2000) describe several possible choices of proposal density. Although the optimal density (minimizing the a posteriori sample variance) $Q(\boldsymbol{X}_k \mid \boldsymbol{X}_{k-1}, \boldsymbol{z}_k) = P(\boldsymbol{X}_k \mid \boldsymbol{X}_{k-1}, \boldsymbol{z}_k)$ can only be determined in very few cases (such as systems with linear measurement equations), approximations using linearization of the measurement equation (such as the extended Kalman particle filter or unscented particle filter; van der Merwe et al. 2000) yield good results. Note that linearization of the measurement equation in order to obtain a proposal density does not imply the disadvantages of Kalman filter linearization techniques. Another way to take into account the information contained in the measurements in the proposal density is by the use of auxiliary variables such as in the ASIR filter (Pitt and Shephard 1999). Sometimes a Markov Chain Monte Carlo (MCMC) transition step (Liu and Chen 1998; MacEachern, Clyde, and Liu 1999) is used to improve the particle filter's performance.

The above problems are worse in the case of parameter estimation and prohibit a fool-proof use of the particle filter. For parameter estimation with particle filters, several alternatives are proposed in the literature, amongst them the use of kernel density estimation methods (Liu and West 2001), the introduction of artificial dynamics on the parameters (Kitagawa 1998; Liu and West 2001), the introduction of an MCMC step (Berzuini and Gilks 2001; Gilks and Berzuini 2001) or the use

5. Note that another inconvenience of the Kalman filter approach is the fact that Kalman filter variants cannot deal with the full system model $P\left(CF_k = j \mid \boldsymbol{X} = \boldsymbol{x}', CF_{k-1} = i\right)$ from eq. (4). Although the presented paper does not use this more accurate but complex system model yet, this would be prohibitive for future research.

6. Because of the on-line estimation requirements, we only consider sampling importance resampling methods for the parameter estimation, and no Markov Chain Monte Carlo or other computationally more intensive methods.

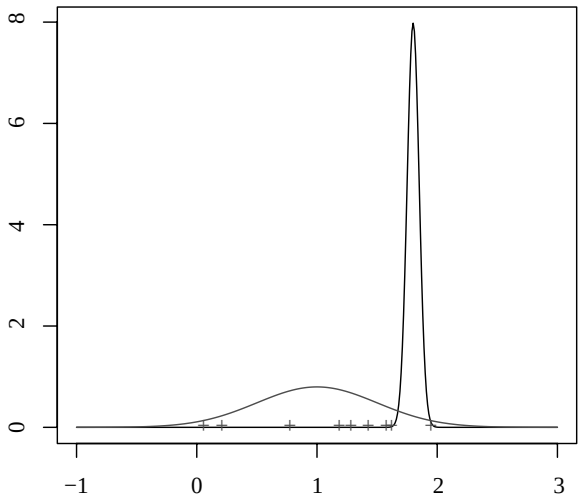

Fig. 3. Illustration of the peaked likelihood problem of particle filters in one dimension. When the likelihood is too peaked, all the samples will have low weights. The problem becomes worse for high-dimensional state spaces and when the initial uncertainty is large.

of particle filters for recursive maximum likelihood (Doucet and Tadic 2003).

4.2.1. Complexity of the Particle Filter Algorithm

Let N be the number of CFs, and M the total number of samples to represent the hybrid joint density. Every continuous estimate belonging to a certain CF $P(\boldsymbol{x}, CF_k = i \mid \boldsymbol{z}_{1\ldots k})$ will be represented by a number of samples M_i proportional to the marginal densities $P(CF_i \mid \boldsymbol{z}_{1\ldots k})$:

$$M_i = P(CF_i \mid \boldsymbol{z}_{1\ldots k}) \times M, \qquad 1 < i < N. \tag{9}$$

The prediction step calculates M samples from the proposal density ($O(M)$). The measurement update multiplies each of the M samples with a weight obtained from the measurement equation. The resampling step draws M_i independent samples from each density $P(\boldsymbol{x}, CF_k = i \mid \boldsymbol{z}_{1\ldots k})$ in $O(M_i)$ (e.g., through ordered uniform sampling; Ripley 1987, p. 96). This means that the total complexity of resampling from the hybrid posterior will always be $O(M)$. Note that the resampling step is optional and can be applied with a fixed period or using a threshold (dynamic resampling).

Consequently, the total time needed for updating the posterior every time-step will be $O(M)$ for a basic particle filter algorithm. Memory requirements are of the same order. Most improved particle algorithms described in the previous section are computationally somewhat more expensive, but remain $O(M)$.

The resulting algorithm, in the case of a simple bootstrap filter with dynamic resampling, is described in algorithm 1. Note that an artificial dynamic is introduced on $\boldsymbol{x}$ to avoid degeneracy.

Algorithm 1. Particle filter algorithm for the hybrid posterior with dynamic resampling and the system model as proposal density.

Sample N samples from the a priori density $P(\boldsymbol{x}_0, CF_0)$
for $i = 1$ to N
  $\tilde{w}_0^i = \frac{1}{N}$
end for
for $k = 0$ to T
  for $i = 1$ to N
    Sample CF_k^i from $P(CF_k \mid CF_{k-1})$
    Sample $\boldsymbol{x}_k^i$ from $P(\boldsymbol{x}_k \mid \boldsymbol{x}_{k-1})$ (artificial dynamic)
    Assign the particle a weight according to the measurement update:
    $w_k^i = P(\boldsymbol{z}_k \mid \boldsymbol{x}_k^i, CF_k^i)\tilde{w}_{k-1}^i$
  end for
  Normalize the weights:
  for $i = 1$ to N
    $\tilde{w}_k^i = \frac{w_k^i}{\sum_{i=1}^N w_k^i}$
  end for
  Calculate the effective sample size $ESS = \frac{1}{\sum_{i=1}^N (\tilde{w}_k^i)^2}$
  if $ESS < threshold$
    Resample
  end if
end for

4.3. Analogy with SLAM

The problem of the simultaneous CF recognition and geometrical parameter estimation is similar to localization for mobile robotics (e.g., SLAM; Thrun, Burgard, and Fox 1998). Although typically the sensors of mobile robots (laser scanners, cameras) yield global information about the environment, and the wrench information coming from a contact is local and less "rich", both solve the so-called "chicken-and-egg" type of estimation problems: often, one cannot separate the model selection from the state/parameter estimation without suffering from divergence problems of the filter due to false assumptions. The Bayesian approach gives a systematic way to cope with simultaneous estimation of both models and states/parameters. The following subsections compare the simultaneous CF recognition and geometrical parameter estimation problem to (i) the data association problem in SLAM problems (Montemerlo and Thrun 2003) and (ii) a mobile robot global localization problem with different models.

4.3.1. Data Association in SLAM

Data association is the problem of assigning measurements to a particular landmark. It is still a major issue (Bar-Shalom and Fortmann 1988; Montemerlo and Thrun 2003; Nieto et al. 2003) in SLAM contexts with fully stochastical or combined stochastical/heuristic methods, such as the nearest-neighbor filter.

Contrary to our research where the recognition of the current CF is of significant importance to be able to choose an appropriate control algorithm, the association of the measurement with the correct landmark is "hidden" in mobile robot localization problems: the mobile robot is not directly interested in the value of this association variable. Still, the problem is important since wrong data associations can lead to a divergence of the filter. Montemerlo and Thrun (2003) describe the FastSLAM algorithm (a Rao–Blackwellized particle filter) with unknown data association and explain why a per-particle maximum likelihood data association is yielding good results. In our case, however, the number of CFs ("landmarks") is fixed and known. Moreover, an erroneous data-association decision might damage the robot or the environment, e.g., in case the robot is velocity controlled in a direction where force control is required. So, in the case of Simultaneous CF recognition and geometrical parameter estimation, a full Monte Carlo data association will yield better results for the variable CF in which we are explicitly interested, since it avoids misclassification due to local maxima problems. Due to the fixed number of CFs, the number of particles does not explode with increasing time-steps. Moreover, a model $P\,(CF_k = j \mid \boldsymbol{X} = \boldsymbol{x}', CF_{k-1} = i)$ is available, predicting the next "landmark". This is only possible if an a priori "map" is available.

4.3.2. Global Localization With Different Models

Simultaneous CF recognition and geometrical parameter estimation is similar to solving a global localization problem in which a robot uses different models (e.g., several different rooms in an office building), but it is uncertain about what model to use (in what room it is). The system graph corresponds to a map of the building and introduces knowledge about the relative location of features that can be used to efficiently solve the problem in the case of Simultaneous CF recognition and geometrical parameter estimation.

In this case, the posterior density (1) denotes the joint probability of being at location $\boldsymbol{X} = \boldsymbol{x}$ in a certain room. Each room has its own particular measurement model. Equation (4) then represents the probability of moving into another room in the building, given the current position of the robot and the inputs to its actuators.

A comparison of the complexity of both problems is very implementation-dependent. Global localization can be performed with five a priori well distinguishable beacons but applications exist where hundreds of natural landmarks are used.

5. Implementation

This section deals with the specific measurement equations for the CF recognition and parameter estimation problem in autonomous compliant motion described in the introduction.

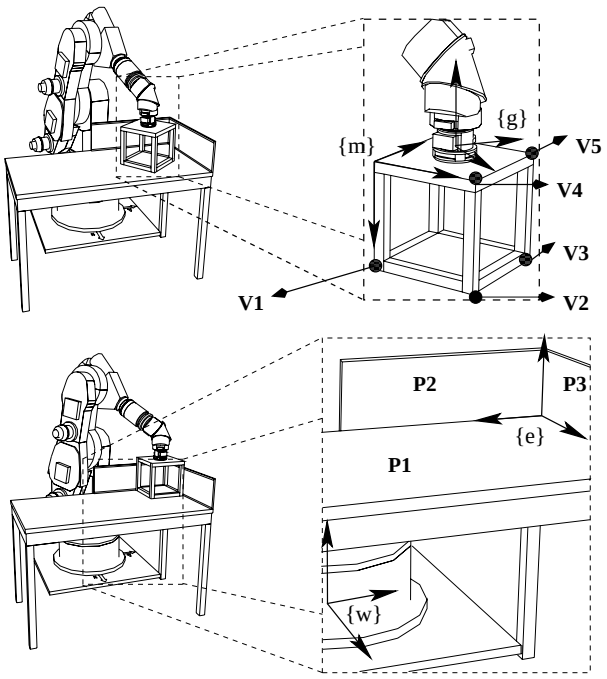

Fig. 4. Frames and vertex/plane numbering for the cube-in-corner experiment: $\{e\}$, $\{w\}$, $\{g\}$, $\{m\}$ denote environment, world, gripper, and MO frame, respectively.

First, Section 5.1 describes the measurement equations for this assembly problem. However, these equations are implicit, and particle filters need explicit equations for the weight update step. The derivation of explicit equations is dealt with in Section 5.2. Finally, Section 5.3 presents a discussion on the modeled uncertainties in the particular case of this assembly task.

5.1. Measurement Equations

Lefebvre, Bruyninckx, and De Schutter (2003a) describe the specific measurement equations of this autonomous compliant motion case in full detail. Therefore, this section focuses on the filter-specific issues of these measurement equations. The definition of the used frames is shown in Figure 4. The parameter vector $\boldsymbol{x}$ is 12-dimensional and contains (i) the position and orientation of the MO (frame $\{m\}$) with respect to the gripper ($\{g\}$) and (ii) the position and orientation of the EO ($\{e\}$) with respect to the world frame ($\{w\}$). The measurement vector contains wrenches (6D), twists (6D) and the position/orientation of the gripper $\{g\}$ with respect to the world frame $\{w\}$.

Each CF can be composed of a number of elementary CFs, e.g., a plane–plane CF can be decomposed into three vertex–plane contacts. This allows automatic generation of the measurement equations for the different CF models (Lefebvre, Bruyninckx, and De Schutter 2003a). Both wrench

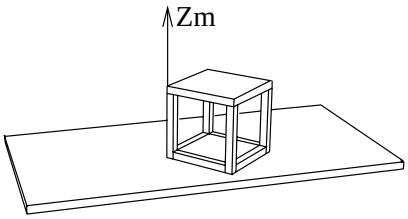

Fig. 5. A single plane–plane contact without friction cannot produce a torque around an axis Zm perpendicular to the planes in contact, nor a force parallel to that plane.

measurements from the force sensor and pose measurements from the encoders give rise to non-linear implicit measurement equations $h(\boldsymbol{x}, \boldsymbol{z}) = \boldsymbol{0}$ (eqs. (10) and (12)).

The wrench measurement equations are based on the approximation that there is no friction during the experiment, and thus the dissipated energy (for each vertex–plane contact) vanishes. For each CF, only a limited subset of the 6D space of wrenches is possible. For example, Figure 5 illustrates that a single plane–plane contact without friction cannot produce a torque around an axis perpendicular to the planes in contact, nor a force parallel to that plane. The vector space of all possible contact wrenches for a certain CF is called the wrench space. Each of those contact wrenches can be written as a linear combination of the vectors in the wrench base $\boldsymbol{G}$. Similarly, a twist base $\boldsymbol{J}$ describes a minimal spanning set for all possible twists in a given CF. Twists and wrenches are reciprocal: in a direction of frictionless motion, one cannot measure a wrench (the dissipated energy vanishes), as expressed by the wrench measurement equation:

$$\boldsymbol{E} = \boldsymbol{J}(\boldsymbol{x})^{\mathrm{T}} \boldsymbol{w} = \boldsymbol{0}. \tag{10}$$

The number of columns of $\boldsymbol{J}$ (and thus the number of rows of the $\boldsymbol{0}$ vector) varies along the given CFs. $\boldsymbol{J}(\boldsymbol{x})$ is a non-linear function of the parameter vector $\boldsymbol{x}$.

The pose measurement equations express the closure of the kinematic chain robot–MO–EO. For example, for a vertex–plane contact this means the vertex lies in the plane and results in

$$\boldsymbol{n}^{\mathrm{T}} \times_e \boldsymbol{p}^{e,c} = d \qquad \text{(one equation per vertex–plane contact)}, \tag{11}$$

where ${}_e\boldsymbol{p}^{e,c}$ is the location of the vertex c expressed in $\{e\}$; and the location of the plane in $\{e\}$ is given by its normal vector $\boldsymbol{n}$ and d is the (perpendicular) distance from the origin of $\{e\}$ to the plane.[7]

Since we only know the position of the vertex in $\{m\}$ we have to transform ${}_m\boldsymbol{p}^{m,c}$ to $\{e\}$. This results in the closure equations

$$\boldsymbol{n} \times_e^w \boldsymbol{T}(\boldsymbol{x}) \times_w^g \boldsymbol{T}(\boldsymbol{z}) \times_g^m \boldsymbol{T}(\boldsymbol{x}) \times_m \boldsymbol{p}^{m,c} = d, \tag{12}$$

where $\boldsymbol{T}$ denotes a non-linear transformation matrix between the different frames.

5.2. Explicit Equations for Particle Filters

Particle filters require explicit measurement equations: at each time-step they calculate the probability of the new measurement $P(\boldsymbol{z}_k \mid \boldsymbol{x})$ for each particle. Kalman filters do not use this probability value. Therefore, it is not possible to use the same measurement equations as in previous research. The following paragraphs explain how the existing implicit measurement equations (constraints) are transformed into explicit equations.

Wrench Measurement Equations. Assuming additive Gaussian uncertainty on the wrench measurements $\boldsymbol{w}$, and taking into account that $\boldsymbol{J}(\boldsymbol{x})$ in eq. (10) is known for a given particle state value $\boldsymbol{x}$, $\boldsymbol{E}$ is a linear transformation of the wrench vector $\boldsymbol{w}$, for a given particle state value $\boldsymbol{x}$. This means that the uncertainty on $\boldsymbol{E}$ also will be additive Gaussian

$$P(\boldsymbol{E} \mid \boldsymbol{x}) = \mathcal{N}(\boldsymbol{0}, \boldsymbol{J}(\boldsymbol{x})^{\mathrm{T}} \boldsymbol{\Sigma}_w \boldsymbol{J}(\boldsymbol{x})), \tag{13}$$

where $\boldsymbol{\Sigma}_w$ denotes the original covariance matrix on $\boldsymbol{w}$ and $\mathcal{N}(\boldsymbol{\mu}, \boldsymbol{\Sigma})$ denotes a multivariate Gaussian with mean value $\boldsymbol{\mu}$ and covariance matrix $\boldsymbol{\Sigma}$. Note that $J(\boldsymbol{x})$ also depends on the pose measurements (due to the frame transformations). However, the uncertainties on the pose measurements are negligible compared to the uncertainties on the wrench measurements.

The "energy measurement vector" $\boldsymbol{E}$ represents the dissipated energy in each of the directions allowing motion freedom. This means the number of rows of $\boldsymbol{E}$ depends on the number of elementary contacts in a given CF and $\boldsymbol{E}$ is a different random variable for each of the CFs. So, it is impossible to compare different CF hypotheses with this approach. However, since wrenches and twists are reciprocal, the combined twist–wrench measurement equation

$$\begin{bmatrix} \boldsymbol{J}^{\mathrm{T}} & \boldsymbol{0} \\ \boldsymbol{0} & \boldsymbol{G}^{\mathrm{T}} \end{bmatrix} \begin{bmatrix} \boldsymbol{w} \\ \boldsymbol{t} \end{bmatrix} = \boldsymbol{0}, \tag{14}$$

where $\boldsymbol{t}$ denotes the twist vector, does represent the "instantaneously dissipated energy" in all possible directions (of dimension six) and can be used to compare different CF hypotheses. Equation (13) then becomes

$$P(\boldsymbol{E} \mid \boldsymbol{x}) = \mathcal{N}\left(\boldsymbol{0}, \begin{bmatrix} \boldsymbol{J}(\boldsymbol{x})^{\mathrm{T}} & \boldsymbol{0} \\ \boldsymbol{0} & \boldsymbol{G}(\boldsymbol{x})^{\mathrm{T}} \end{bmatrix}^{\mathrm{T}} \begin{bmatrix} \boldsymbol{\Sigma}_w & \boldsymbol{0} \\ \boldsymbol{0} & \boldsymbol{\Sigma}_t \end{bmatrix} \begin{bmatrix} \boldsymbol{J}(\boldsymbol{x})^{\mathrm{T}} & \boldsymbol{0} \\ \boldsymbol{0} & \boldsymbol{G}(\boldsymbol{x})^{\mathrm{T}} \end{bmatrix}\right), \tag{15}$$

where $\boldsymbol{\Sigma}_t$ denotes the original covariance matrix on $\boldsymbol{t}$.

7. Written down in a scalar form, eq. (11) is equivalent to $ax+by+cz-d=0$, where $\boldsymbol{n}^{\mathrm{T}} = [a\ b\ c]$ is normal to the plane and the coordinates of the vertex in the appropriate frame are $[x\ y\ z]^{\mathrm{T}}$.

Pose Measurement Equations. The closure equations (12) express the fact that, per vertex–plane contact, the perpendicular distance from the vertex to the plane should vanish. These equations are implicit, suggesting the application of a technique similar to that used in the above paragraph, with the perpendicular distance to the plane d as a new, "derived" measurement variable. However, unlike in the case of the twist–wrench measurement eq. (14), for a given value of $\boldsymbol{x}$, the transformation between the pose measurement (denoted as $\boldsymbol{z}$ in eq. (12)) and d is still non-linear. This means that additive Gaussian uncertainty on the pose measurements will no longer be additive Gaussian uncertainty on the transformed distance measurement.

The original choice of adding additive Gaussian uncertainty to the pose measurements in previous research was due to the fact that additive Gaussian uncertainty is a necessary assumption for the Kalman filter. This assumption is justified by the central limit theorem, which states that any sum of many independent identically distributed random variables is approximately normally distributed. The uncertainty is the sum of (i) position errors on the six joint positions of the robot, (ii) the compliance of the MO, EO, and force sensor, (iii) measurement noise and discretization errors in the encoders, and (iv) errors in the kinematics. Since this assumption also holds for the perpendicular distance d from the origin of $\{e\}$ to the plane, adding Gaussian uncertainty to the distance vector instead of the pose measurement vector is justifiable.

A second problem with this transformation is the difference in dimensions of the transformed measurement vector between different CFs. For each vertex plane contact, an equation of the form (12) can be written. The solution is found by treating all CFs as combinations of vertex–plane contacts: e.g., for a single plane–plane (SPP) contact the following holds during the cube-in-corner assembly

$$P(CF = \text{SPP}) = P(\text{V1 in P1, V2 in P1, V3 in P1,}$$
$$\text{V4 } \textbf{not} \text{ in P2, V5 } \textbf{not} \text{ in P2, V5 } \textbf{not} \text{ in P3}) \tag{16}$$

where Vi denotes vertex i and Pj denotes plane j, as shown in Figure 4. For each individual vertex plane contact, we assume

$$P(d \mid \boldsymbol{x}, \text{V}i \text{ in P}j) = \mathcal{N}(d_j, \sigma_{ij}). \tag{17}$$

Note that σ_{ij} could depend on $\boldsymbol{x}$. d_j denotes the perpendicular distance from the origin of $\{e\}$ to plane j. If Vi is not in Pj, we assume d is also normally distributed, but with a another mean value d'_j and another covariance matrix. So, if the vertex is not in contact with the plane, we have

$$P(d \mid \boldsymbol{x}, \text{V}i \text{ not in P}j) = \mathcal{N}(d'_j, \sigma'_{ij}). \tag{18}$$

Note that d'_j is not equal to d_j, and will depend on $\boldsymbol{x}$.

For each CF, we can construct a measurement vector from r transformed pose measurements (r is the minimal number of single vertex–plane contacts in the most constrained CF, and $r = 6$ in the case of the cube-in-corner application). The resulting probability is the product of the "individual" Gaussian probabilities, e.g., for a single plane–plane contact:

$$\begin{aligned} P(\boldsymbol{z}' \mid \boldsymbol{x}, CF_k = SPP) &= P(d_1 \mid \boldsymbol{x}, CF_k = SPP) \\ &\quad P(d_2 \mid \boldsymbol{x}, CF_k = SPP) \ldots \\ &\quad P(d_5 \mid \boldsymbol{x}, CF_k = SPP) \\ &= P(d_1 \mid \boldsymbol{x}, V1 \text{ in } P1) \\ &\quad P(d_2 \mid \boldsymbol{x}, V2 \text{ in } P1) \ldots \\ &\quad P(d_5 \mid \boldsymbol{x}, V5 \text{ not in } P3). \end{aligned} \tag{19}$$

5.3. Uncertainty on the Models

The pose uncertainty originating from the (calibrated) robot is much smaller than the uncertainty on the wrench measurements. This is due to the nature of the wrench sensor and the model errors (such as friction) in the wrench measurement model. Therefore, the stochastical estimator mainly uses the information of pose measurements for its estimation of the geometrical parameters, i.e., the uncertainty on the pose measurements determines the accuracy of the estimates of the geometrical parameters.

Previous research (Lefebvre, Bruyninckx, and De Schutter 2003a) used wrench measurements mainly to detect CF transitions. It only took into account the possibility of a CF transition when the SNIS-test failed, due to an inconsistency of wrench–twist measurements with the model. This research also uses the pose models to detect CFs.

6. Experimental Results

In this section we describe the experimental results of the estimation of geometrical parameters and CFs with a particle filter. The established CFs during the experiment are the vertex–plane CF (CF0), the edge–plane CF (CF1), the plane–plane CF (CF2), the plane–plane + edge–plane CF (CF3), the two plane–plane CF (CF4) and the three plane–plane CF (CF5).

At time 0, we know for sure that the cube is in free space ($P(CF_0 = CF0) = 1$). We suppose $P(\boldsymbol{X} = x \mid CF_0 = CF0)$ is a multivariate Gaussian, with the initial values as described in Lefebvre, Bruyninckx, and De Schutter (2003a) to allow comparison of the results; the parameters of the MO and EO are uncorrelated. The chosen means are

$$\begin{aligned} \mu_{EO_\theta} &= [-0.07 \ -0.06 \ -3.2]^{\text{T}}, \\ \mu_{EO_{pos}} &= [0.4 \ -0.65 \ -0.75]^{\text{T}}, \\ \mu_{MO_\theta} &= [0.01 \ 0.01 \ -0.78]^{\text{T}}, \\ \mu_{MO_{pos}} &= [0.122 \ 0.127 \ -0.0155]^{\text{T}} \end{aligned}$$

(rotations expressed in radians, positions in m). The true values of the parameters were

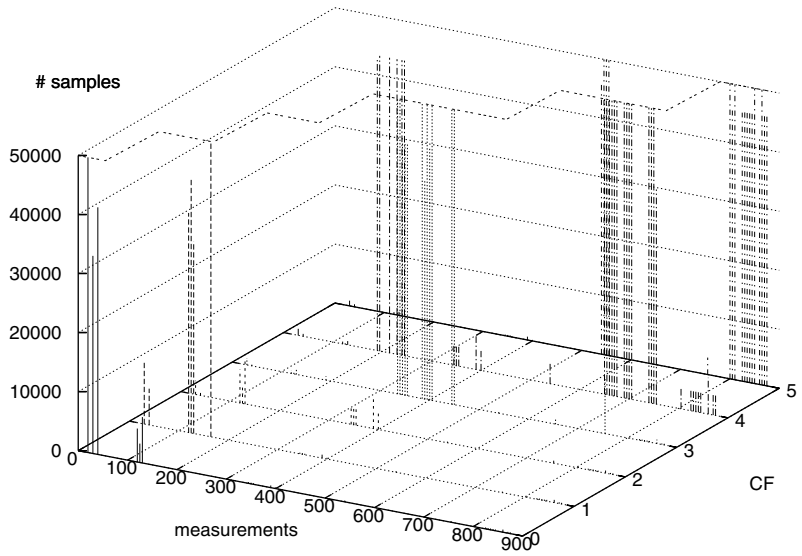

Fig. 6. True CF evolution (top dashed-line curve) and sample-based estimate using a bootstrap filter with 50,000 samples. The "meas" axis denotes the number of the processed measurements, the "# samples" axis shows the number of samples in a particular CF. So a cross-section parallel to the plane formed by the "# samples" and the "CF" axis, and crossing the "meas" axis at time k, represents the marginal posterior density $P(CF_k = i|z_{1\ldots k})$. Similar results are obtained using a particle filter with as few as 100 samples.

$$\mu_{EO_\theta} = [0\ 0\ -3.1415]^{\mathrm{T}},$$
$$\mu_{EO_{pos}} = [0.457\ -0.608\ -0.680]^{\mathrm{T}},$$
$$\mu_{MO_\theta} = [0\ 0\ -0.785]^{\mathrm{T}},$$
$$\mu_{MO_{pos}} = [0.125\ 0.125\ -0.015]^{\mathrm{T}}.$$

The chosen covariances for rotational uncertainty are (in degrees)

$$\Sigma_{EO_\theta} = \begin{bmatrix} (10^\circ)^2 & 0 & 0 \\ 0 & (10^\circ)^2 & 0 \\ 0 & 0 & (10^\circ)^2 \end{bmatrix}, \quad \Sigma_{MO_\theta} = \begin{bmatrix} (1^\circ)^2 & 0 & 0 \\ 0 & (1^\circ)^2 & 0 \\ 0 & 0 & (1^\circ)^2 \end{bmatrix}.$$

For position uncertainty, we chose

$$\Sigma_{EO_{pos}} = \begin{bmatrix} (100\ \mathrm{mm})^2 & 0 & 0 \\ 0 & (100\ \mathrm{mm})^2 & 0 \\ 0 & 0 & (100\ \mathrm{mm})^2 \end{bmatrix}, \quad \Sigma_{MO_{pos}} = \begin{bmatrix} (1\ \mathrm{mm})^2 & 0 & 0 \\ 0 & (1\ \mathrm{mm})^2 & 0 \\ 0 & 0 & (1\ \mathrm{mm})^2 \end{bmatrix}.$$

In Section 6.1 we describe the results of the CF recognition using only the twist and wrench measurement, and in Section 6.2 we describe the results of both CF recognition and parameter estimation when using both measurement models.

6.1. CF Estimation Using Only Twist and Wrench Data

Using only the information from the twist and (noisy) wrench data, the particle filter cannot estimate the geometrical parameters but should be able to recognize the different CFs. Figure 6 shows the results of a C++ program with 50,000 samples, using the Bayesian Filtering Library (see Section 7) on a 1.13 GHz/128 Mbytes RAM pc, running Linux.[8] An artificial dynamic was introduced on the parameters to avoid degeneracy problems (Kitagawa 1998; Liu and West 2001). The resulting algorithm is that described in algorithm 1.

Figure 6 illustrates that the particle filter estimates the CF reasonably well when contacts are well established (otherwise no model is available), except in the plane–plane CF (CF2, between measurements 180 and 280) and a part of the two plane–plane CF (between measurements 506 and 560). Both "errors" can be explained given the values of the twist measurements during those periods (Figure 7). The particle filter identifies the plane–plane CF as a two plane–plane contact. This is caused by the fact that the angular velocities in the extra degrees of freedom of the plane–plane CF (with respect to the two plane–plane contact) are virtually zero. The plane–plane CF allows a rotation around the axis perpendicular to the plane (denoted as the "Rot z" in Figure 7) but the robot does not use this degree of freedom. So, based on these measurements, it is not possible to distinguish between the plane–plane (CF2, contact measurements 172–284) and the

8. For this problem, the same results were obtained with as few as 100 particles. One inconvenience of particle filters is the fact that, to the best of our knowledge, there is currently no algorithm that can predict how many samples must be applied in order to achieve meaningful results using a particle filter. The only solution is trial and error. Without any optimizations, ±500 samples can be used to process the measurements at a rate of 10 Hz.

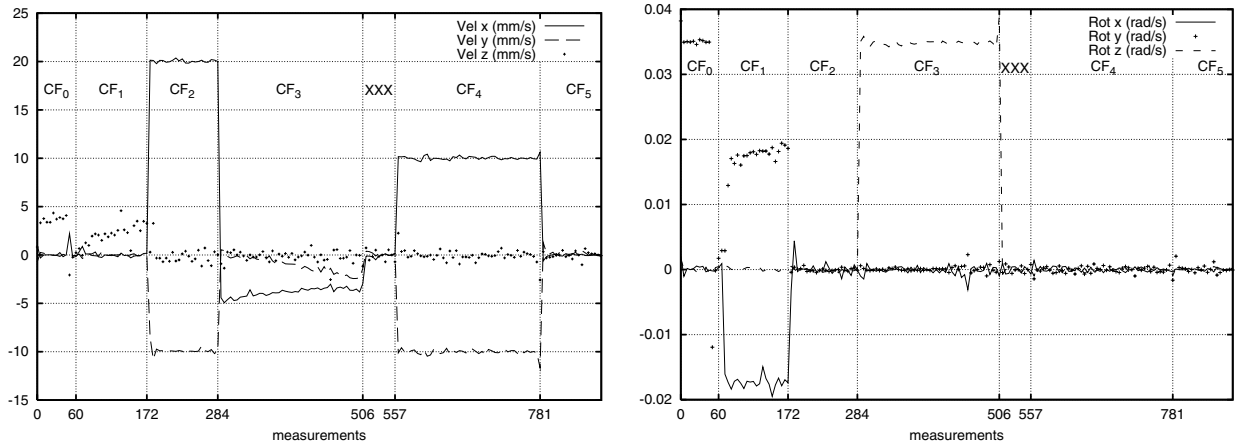

Fig. 7. Translational and angular velocity measurements during cube-in-corner experiment. The XXX denotes the part of CF3 where the robot does not move.

two plane–plane contact (CF4, measurement 557–781) given only the twist measurements. Occam's razor (Jeffreys 1939) then explains why the particle filter assigns more probability to the two plane–plane CF by looking at the difference in the covariance on $\boldsymbol{E}$ between the two CFs. Due to the much higher uncertainty, wrench measurements are not significantly present in the filter's estimates. As an example, suppose the current CF is the free space contact. This CF has a twist base $\boldsymbol{J}$ of six columns and an empty wrench base. Equation (15) is then equivalent to eq. (13). The resulting covariance matrix on $\boldsymbol{E}$ will be large, since the covariance matrix on $\boldsymbol{w}$ is also large (compared to the covariance on the twist measurements). On the other hand, consider the three plane–plane CF: $\boldsymbol{J}$ is now empty, whereas the wrench basis $\boldsymbol{G}$ consists of six columns. So, eq. (15) simplifies to $P(\boldsymbol{E} \mid \boldsymbol{x}) = \mathcal{N}(\boldsymbol{0}, \boldsymbol{G}(\boldsymbol{x})^{\mathrm{T}} \boldsymbol{\Sigma}_t \boldsymbol{G}(\boldsymbol{x}))$. The covariance matrix on $\boldsymbol{E}$ is smaller, since the covariance matrix on $\boldsymbol{t}$ is small compared to the covariance on the wrench measurements (and $\boldsymbol{J}$ and $\boldsymbol{G}$ are of the same order of magnitude). For one dimension, this is shown in Figure 8. If velocities in certain directions are low, both CFs explain these measurements. Occam's razor will prefer the "simpler" model with the smaller covariance.

The error during the two plane–plane CF (identified by the particle filter as a three plane–plane CF) is also explained using Occam's razor given the fact that the robot does not move at all during this time period (see Figure 7 during measurements 506–557).

When increasing the initial uncertainty a lot, we notice the same tendency to favor CFs with fewer degrees of freedom. This would not happen if (i) the uncertainty on the wrench measurements was smaller (e.g., if a friction model were available), and/or (ii) the motion degrees of freedom were better excited (for the first situation).

The effect of changing the parameters of the system model is minor, suggesting that the information contained in the measurements is rich enough to compensate the approximate system model of Section 3. The presented results are obtained using the following transition matrix:

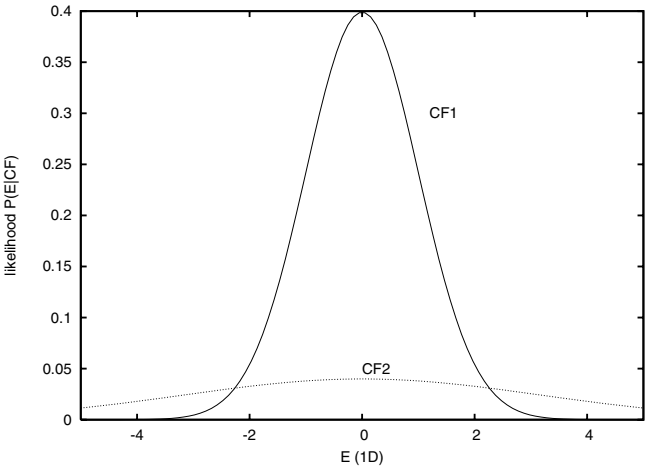

Fig. 8. One-dimensional illustration of Occam's razor principle. CF1 corresponds to a CF with a small covariance matrix, CF2 to a CF with a larger covariance matrix. If the measurement's value is around 0, both models explain it, but CF1 will be preferred.

$$\begin{bmatrix} 0.95 & 0.03 & 0.005 & 0.005 & 0.005 & 0.005 \\ 0.02 & 0.95 & 0.02 & 0.0033 & 0.0033 & 0.0033 \\ 0.0033 & 0.02 & 0.95 & 0.02 & 0.0033 & 0.0033 \\ 0.0033 & 0.0033 & 0.02 & 0.95 & 0.02 & 0.0033 \\ 0.0033 & 0.0033 & 0.0033 & 0.02 & 0.95 & 0.02 \\ 0.005 & 0.005 & 0.005 & 0.005 & 0.03 & 0.95 \end{bmatrix}.$$

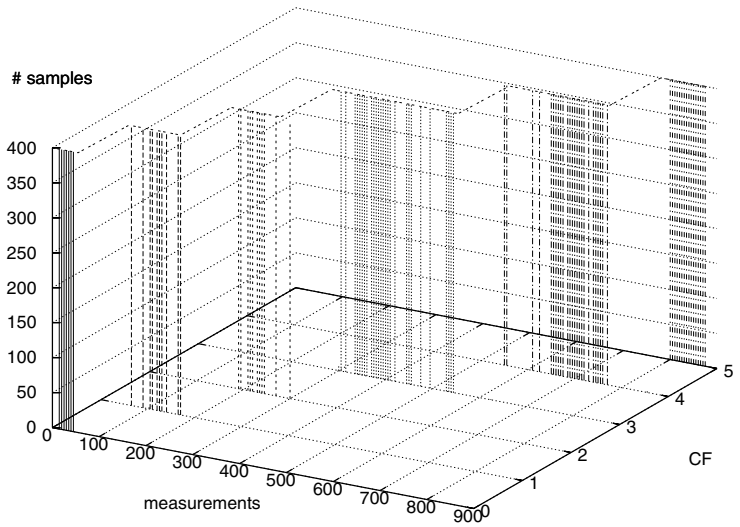

Fig. 9. CF recognition with information from both measurement models.

6.2. Simultaneous Geometrical Parameter Estimation and CF Recognition Using Position and Wrench Twist Information

6.2.1. CF Recognition

Implementing the pose measurement model described in Section 5.2 requires the choice of parameters μ and σ in both eqs. (17) and (18). Although a very rough approximation of reality,[9] we chose

$$d'_j = d_j, \tag{20}$$

where d_j is the (perpendicular) distance of plane Pj to the origin of the environment frame $\{e\}$ and

$$\sigma_{ij}^2 = (2\text{ mm})^2 \qquad (\sigma')_{ij}^2 = (300\text{ mm})^2. \tag{21}$$

These approximations appear sufficient (again, using Occam's razor principle) to distinguish between the two situations (in contact or not) and to estimate (a part of) the geometrical parameter vector if Vi is in contact with Pj. Figure 9 shows the result of such a simulation with 400 samples. The complementary information in both measurement models allows us to estimate the CF far better than using only the twist–wrench model. Indeed, in the two cases described above, the extra information stemming from the position measurements allows us to choose the right CF. Note also that, compared to Figure 6, the marginal posterior density at time-step k, $P(CF_k|z_{1\ldots k})$, is far less "spread out" along the CF-axis. This is logical due to the relative quality of the position measurements with respect to the wrench/twist information.

9. In reality, the mean distance d_j and the covariance σ_{ij}^2 will be dependent of i and j (the indices of vertex and plane in contact, respectively). So, using only position information and the approximative values in those equations, a transition in CF is made sometimes too soon, sometimes too late. So, only the combination of the force/twist and position allows us to perform the CF recognition "seamlessly".

6.2.2. Geometrical Parameter Estimation

Using information of both measurement models, the particle filter also provides estimates for the geometrical parameters. Figure 10 shows the results for the geometrical parameter estimates of the EO, obtained by marginalizing the hybrid posterior from the particle filter. The algorithm yields similar results as provided by an IEKF, where the segmentation and CF detection still was done manually. Note that not all parameters are observable in all CFs, e.g., a single vertex–plane contact does not yield any information about x^e, y^e, or θ_z^e. This explains why most estimates only converge to the true values after a large number of measurements. For this particular case, running the (non-optimized) algorithm with 5000 samples (which are necessary to provide a reasonable good estimate of the geometrical parameters) takes about 1500 s on a 1.1 GHz laptop (to process the 900 measurements). This means that an optimized version of the code could easily process measurements at a rate of 1 Hz. Furthermore, since algorithm 1 used a basic particle filter with a simple proposal density, using better proposal densities would lead to significant improvements in accuracy (or obtaining the same accuracy faster with less particles). This is a topic of future research.

7. Software

The Free Software Bayesian Filtering library (http://people.mech.kuleuven.ac.be/~kgadeyne/bfl.html) offers a unifying framework for all Bayesian filters. Since it should be possible to use the library in (hard or soft) real time, a recursive

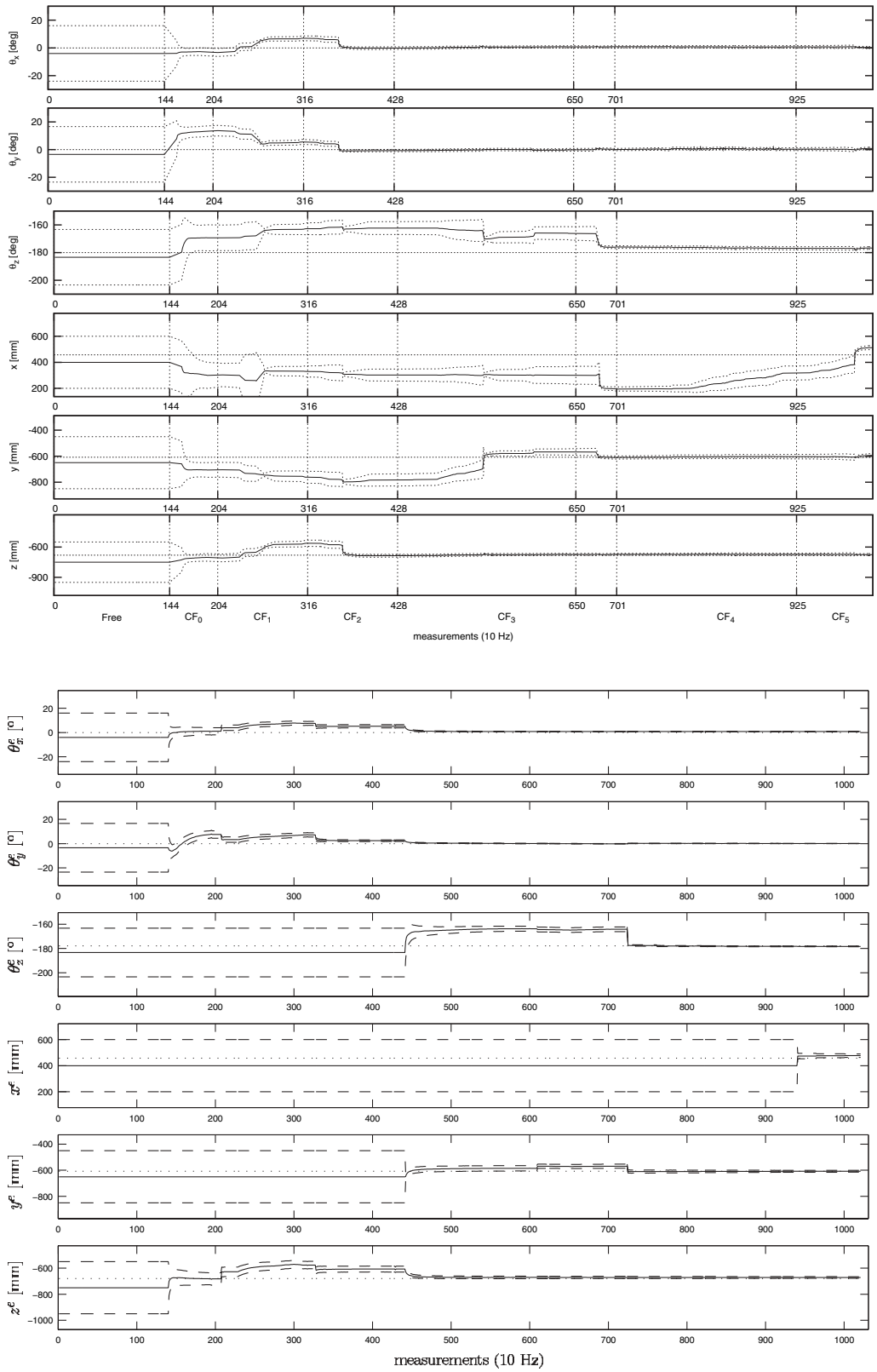

Fig. 10. Top: particle filter estimates of the geometrical parameters of the EO. The straight horizontal dotted line denotes the true parameter. The full line shows the posterior mean of the particle filter and the curved dashed lines denote the 2σ boundary. 50,000 samples were used for this figure; 5000 samples are sufficient to assure convergence. Bottom: IEKF estimates with manual segmentation of CFs.

approach (assuming Markovian systems) is necessary to assure fixed-time computation. The main concepts of this C++ library are (i) the concept of a PDF, allowing to distinguish the notion of a PDF from its representation (i.e., sample-based or analytic form), (ii) the concept of a system and measurement model, independent of, but applicable to, all filters, and (iii) a wrapper numerical library to avoid dependence on a specific library. This design allows us to compare the performance of different filters on the same problem with a maximum code reuse.

The library was primarily designed to serve in robotic state estimation problems, but is independent of any particular application and can therefore be used in a broad range of domains such as mobile robotics, econometrics, actuarial sciences, etc.

8. Summary and Conclusions

In this paper we have presented simultaneous model-based estimation of geometrical parameters and CF recognition in environments with a significant amount of uncertainty. Previous research (Lefebvre, Bruyninckx, and De Schutter 2003a) only used wrench measurements to detect CF transitions. This work develops a hybrid (partly discrete, partly continuous) approach, using an explicit discrete transition model for CFs where both pose and wrench measurements are used to detect CFs. This allows us to deal with larger uncertainties in both CF and continuous geometrical parameter estimation. We argue that Kalman filter variants, used in previous research for the estimation of geometrical parameters given a certain model, are not able to cope with this increased level of complexity. Indeed, the IEKF can only handle small uncertainties due to the non-linearities in the models, and the NMSKF cannot deal with model selection. Particle filter implementations successfully estimate the hybrid posterior density. The CF recognition problem is similar to the data association problem in SLAM-like applications, but there is a major difference: in mobile robot localization problems, the mobile robot controller is not directly interested in the value of the "data association" variable, while for force-controlled assembly that value is of utmost importance in order to select a safe control law that fits with the current contact constraints. We advocate the use of a hybrid posterior instead of the popular maximum likelihood approach in mobile robotics for this particular problem, due to the nature of the compliant motion problem and the importance of a correct contact recognition. Explicit measurement models for the particle filter, based on energetic and closure constraints, are developed, leading to good experimental results for both the CF recognition and the estimates of the 12-dimensional parameter vector. The increased complexity due to the use of the hybrid posterior is acceptable for this particular case.

Ongoing research focuses on the following.

- The use of better models for the description of the transition behavior between CFs.
- A better choice of proposal distribution of the particle filter (local linearization of measurement model), taking into account the last measurement such as the extended Kalman particle filter or the unscented particle filter.
- Active sensing is also envisioned, i.e., imposing motion trajectories and CF transitions to speed up the estimation of the geometrical parameters to a desired accuracy.

Acknowledgments

The authors gratefully acknowledge the financial support by K. U. Leuven's Concerted Research Action GOA/99/04. They wish to thank two anonymous reviewers for their valuable comments on the first version of this paper.

References

Asada, H. 1993. Representation and learning of nonlinear compliance using neural nets. *IEEE Transactions on Robotics and Automation* 9(6):863–867.

Bar-Shalom, Y. and Fortmann, T. E. 1988. *Tracking and Data Association*. Mathematics in Science and Engineering. Academic Press, New York.

Bar-Shalom, Y. and Li, X. 1993. *Estimation and Tracking, Principles, Techniques, and Software*, Artech House, Boston, MA.

Berzuini, C. and Gilks, W. 2001. RESAMPLE–MOVE filtering with cross–model jumps. *Sequential Monte Carlo Methods in Practice*, A. Doucet, N. de Freitas, and N. Gordon, editors, Springer-Verlag, Berlin, pp. 117–138.

Debus, T., Dupont, P., and Howe, R. 2002. Contact state estimation using multiple model estimation and hidden Markov models. *Proceedings of the International Symposium on Experimental Robotics*, Sant'Angelo d'Ischia, Italy.

De Schutter, J. and Van Brussel, H. 1988. Compliant motion I, II. *International Journal of Robotics Research* 7(4):3–33.

De Schutter, J., Bruyninckx, H., Dutré, S., De Geeter, J., Katupitiya, J., Demey, S., and Lefebvre, T. 1999. Estimating first-order geometric parameters and monitoring contact transitions during force-controlled compliant motions. *International Journal of Robotics Research* 18(12):1161–1184.

Doucet, A. and Tadic, V. B. 2003. Parameter estimation in general state-space models using particle methods. *Annals of the Institute of Statistical Mathematics* 55(2):409–422.

Doucet, A., Godsill, S., and Andrieu, C. 2000. On sequential Monte Carlo sampling methods for Bayesian filtering. *Statistics and Computing* 10(3):197–208.

Doucet, A., de Freitas, N., and Gordon, N., editors. 2001. *Sequential Monte Carlo Methods in Practice*. Statistics for engineering and information science. Springer-Verlag, Berlin.

Eberman, B. 1997. A model-based approach to Cartesian manipulation contact sensing. *International Journal of Robotics Research* 16(4):508–528.

Gadeyne, K. and Bruyninckx, H. 2001. Markov techniques for object localization with force-controlled robots. *Proceedings of the International Conference on Advanced Robotics*, Budapest, Hungary, pp. 91–96.

Gilks, W. R. and Berzuini, C. 2001. Following a moving target—Monte Carlo inference for dynamic Bayesian models. *Journal of the Royal Statistical Society* 63(Part 1):127–146.

Gordon, N., Salmond, D. J., and Smith, A. F. M. 1993. Novel approach to nonlinear/non-Gaussian state estimation. *IEE Proceedings F* 140(2):107–113.

Hannaford, B. and Lee, P. 1991. Hidden Markov model analysis of force/torque information in telemanipulation. *International Journal of Robotics Research* 10(5):528–539.

Hirukawa, H., Papegay, Y., and Matsui, T. 1994. A motion planning algorithm for convex polyhedra in contact under translation and rotation. *Proceedings of the International Conference on Robotics and Automation*, San Diego, CA, May, pp. 3020–3027.

Hovland, G. E. and McCarragher, B. J. 1998. Hidden Markov models as a process monitor in robotic assembly. *International Journal of Robotics Research* 17(2):153–168.

Jeffreys, H. 1939. *Theory of Probability*, Clarendon Press, Oxford. (1948, 2nd edition; 1961, 3rd edition; 1998, reprinted by Oxford University Press).

Kalman, R. E. 1960. A new approach to linear filtering and prediction problems. *Transactions of the ASME, Journal of Basic Engineering* 82:34–45.

Kitagawa, G. 1998. A self-organizing state-space model. *Journal of the American Statistical Association* 93(443):1203–1215.

Lefebvre, T. 2003. Contact modelling, parameter identification and task planning for autonomous compliant motion using elementary contacts. Ph.D. Thesis, Katholieke Universiteit Leuven, May.

Lefebvre, T., Bruyninckx, H., and De Schutter, J. 2003a. Polyhedral contact formation modeling and identification for autonomous compliant motion. *IEEE Transactions on Robotics and Automation* 19(3):26–41.

Lefebvre, T., Bruyninckx, H., and De Schutter, J. 2003b. Kalman filters for nonlinear systems: a comparison of performance. *International Journal of Control* 77(7):639–653.

Lefebvre, T., Bruyninckx, H., and De Schutter, J. 2004. Exact nonlinear Bayesian parameter estimation for autonomous compliant motion. *Advanced Robotics* 18(8):787–800.

Lefebvre, T., Bruyninckx, H., and De Schutter, J. 2005. Polyhedral contact formation identification for autonomous compliant motion: exact nonlinear Bayesian filtering. *IEEE Transactions on Robotics and Automation* 21(1):124–129.

Liu, J. S. and Chen, R. 1998. Sequential Monte Carlo methods for dynamic systems. *Journal of the American Statistical Association* 93(443):1032–1044.

Liu, J. S. and West, M. 2001. Combined parameter and state estimation in simulation-based filtering. *Sequential Monte Carlo Methods in Practice*, A. Doucet, N. de Freitas, and N. Gordon, editors, Springer-Verlag, Berlin, pp. 197–223.

MacEachern, S. N., Clyde, M. A., and Liu, J. S. 1999. Sequential importance sampling for non-parametric Bayes models: the next generation. *Canadian Journal of Statistics* 27(2):251–267.

Mihaylova, L., Lefebvre, T., Staffetti, E., Bruyninckx, H., and De Schutter, J. 2002. Contact transitions tracking during force-controlled compliant motion using an interacting multiple model estimator. *Information and Security* 9:114–129.

Mimura, N. and Funahashi, Y. 1994. Parameter identification of contact conditions by active force sensing. *Proceedings of the International Conference on Robotics and Automation*, San Diego, CA, pp. 2645–2650.

Montemerlo, M. and Thrun, S. 2003. Simultaneous localization and mapping with unknown data association. *Proceedings of the International Conference on Robotics and Automation*, Taipei, Taiwan, pp. 1985–1991.

Montemerlo, M., Thrun, S., Koller, D., and Wegbreit, B. 2002. FastSLAM: a factored solution to the simultaneous localization and mapping problem. *Proceedings of the National Conference on Artificial Intelligence*, Edmonton, Alberta, Canada, pp. 593–598.

Murphy, K. P. and Russell, S. 2001. Rao–Blackwellized particle filtering for dynamic Bayesian networks. *Sequential Monte Carlo Methods in Practice*, A. Doucet, N. de Freitas, and N. Gordon, editors, Springer-Verlag, Berlin, pp. 499–516.

Nieto, J., Guivant, J., Nebot, E., and Thrun, S. 2003. Real-time data association for FastSLAM. *Proceedings of the International Conference on Robotics and Automation*, Taipei, Taiwan, pp. 412–418.

Pitt, M. and Shephard, N. 1999. Filtering via simulation: auxiliary particle filters. *Journal of the American Statistical Association* 94(446):590–599.

Ripley, B. D. 1987. *Stochastic Simulation*, Wiley, New York.

Skubic, M. and Volz, R. 2000. Identifying single-ended contact formations from force sensor patterns. *IEEE Transactions on Robotics and Automation* 16(5):597–603.

Slaets, P., Rutgeerts, J., Gadeyne, K., Lefebvre, T., Bruyninckx, H., and De Schutter, J. 2004. Construction of a geometric 3D model from sensor measurements collected during compliant motion. *Proceedings of the International Symposium on Experimental Robotics*, Singapore, in press.

Thrun, S., Burgard, W., and Fox, D. 1998. A probabilistic approach to concurrent mapping and localization for mobile robots. *Machine Learning and Autonomous Robots* 31:29–53.

van der Merwe, R., Doucet, A., de Freytas, N., and Wan, E. 2000. The Unscented Particle Filter. Technical Report CUED/F-INFENG/TR 380, Cambridge University Engineering Department, Cambridge, UK, August.

Xiao, J. and Ji, X. 2001. On automatic generation of high-level contact state space. *International Journal of Robotics Research* 20(7):584–606.